



Article

Electrosprayed Ultra-Thin Coating of Ethyl Cellulose on Drug Nanoparticles for Improved Sustained Release

Wei-Dong Huang ^{1,2,†}, Xizi Xu ^{3,†}, Han-Lin Wang ², Jie-Xun Huang ², Xiao-Hua Zuo ¹,
Xiao-Ju Lu ^{1,*}, Xian-Li Liu ^{2,*} and Deng-Guang Yu ^{3,*}

¹ School of Chemistry and Chemical Engineering, Hubei Polytechnic University, Huangshi 435003, China; neweydong@hbpu.edu.cn (W.-D.H.); 211005@hbpu.edu.cn (X.-H.Z.)

² Hubei Key Laboratory of Mine Environmental Pollution Control and Remediation, School of Environmental Science and Engineering, Hubei Polytechnic University, Huangshi 435003, China; 211041@hbpu.edu.cn (H.-L.W.); huangjiexun@hbpu.edu.cn (J.-X.H.)

³ School of Materials Science and Engineering, University of Shanghai for Science and Technology, Shanghai 200093, China; 192432592@st.usst.edu.cn

* Correspondence: luxiaoju@hbpu.edu.cn (X.-J.L.); liuxianli@hbpu.edu.cn (X.-L.L.); ydg017@usst.edu.cn (D.-G.Y.); Tel.: +86-714-6348814 (X.-J.L.); +86-714-6368937 (X.-L.L.); +86-21-55270632 (D.-G.Y.)

† These authors contributed equally to this work.

Received: 15 August 2020; Accepted: 4 September 2020; Published: 6 September 2020



Abstract: In nanopharmaceutics, polymeric coating is a popular strategy for modifying the drug release kinetics and, thus, new methods for implementing the nanocoating processes are highly desired. In the present study, a modified coaxial electro spraying process was developed to formulate an ultra-thin layer of ethyl cellulose (EC) on a medicated composite core consisting of tamoxifen citrate (TAM) and EC. A traditional single-fluid blending electro spraying and its monolithic EC-TAM nanoparticles (NPs) were exploited to compare. The modified coaxial processes were demonstrated to be more continuous and robust. The created NPs with EC coating had a higher quality than the monolithic ones in terms of the shape, surface smoothness, and the uniform size distribution, as verified by the SEM and TEM results. XRD patterns suggested that TAM presented in all the NPs in an amorphous state thanks to the fine compatibility between EC and TAM, as indicated by the attenuated total reflection (ATR)-FTIR spectra. In vitro dissolution tests demonstrated that the NPs with EC coating required a time period of 7.58 h, 12.79 h, and 28.74 h for an accumulative release of 30%, 50%, and 90% of the loaded drug, respectively. The protocols reported here open a new way for developing novel medicated nanoparticles with functional coating.

Keywords: coaxial electro spraying; surface design; coating process; sustained release; release kinetic; nanoparticles

1. Introduction

During the past several decades, polymeric excipients have provided numerous strategies for developing new dosage forms with all sorts of drug-controlled release profiles [1–4]. Among them, polymeric coating is one of the most popular strategies for modifying the drug release kinetics in both the traditional pharmaceutical industry and also the advanced laboratory nanomethods [5–13]. Particularly in nanopharmaceutics, the simple and robust nanocoating methods are highly desired [14–18]. In general, there are two kinds of nanofabrication routes, i.e., bottom-up and top-down [19–21]. The bottom-up routes (such as molecular self-assembly) have their advantages in production,

such as accurate manipulation and adjusting of the products' sizes. However, they often comprise time-consuming and multiple-step processes and, thus, often have the difficulties of production on a large scale [22]. In comparison, the top-down routes (such as electrospinning and electrospraying) hold the fine promises for creating nanoproducts in a single-step manner and on a large scale [23–32] and, thus, they should provide new strategies for implementing nanocoating on solid medicated nanoparticles [33–37].

In a broad meaning, the coating of polymer on a medicated core represents a shell section of a core-shell structure [38–43]. Electrospinning, as a brother technique of electrospraying, has broadly demonstrated its great power in creating core-shell nanofibers [44,45]. In literature, coaxial electrospinning [44–46], modified coaxial electrospinning [46], modified triaxial electrospinning [47–50], and other complicated processes [51] are reported to generate a thin layer of coating on the core medicated nanofibers. The created core-shell nanostructures with a polymer nanocoating are verified to be very useful for manipulating the drug-loading amount and also their sustained release profiles. Enlightened by electrospinning, electrospraying (particularly the coaxial electrospraying) should play its important role in creating nanocoating on the solid medicated nanoparticles.

For a successful coaxial electrospraying, the traditional concept is that the shell working fluid must be solidifiable (meaning that solid particles can be produced after being subjected to a single-fluid electrospraying process) to form a solid core-shell nanostructure; the core fluid either has or does not have solidifiable properties. This knowledge was achieved from the first study about traditional coaxial electrospraying [52]. However, Liu et al. successfully demonstrated a modified coaxial electrospraying process, in which the shell fluid was unsolidifiable organic solvent. The shell solvent changed the interfaces between the atmosphere and the polymeric working fluid through inserting a middle solvent layer during the spraying process. The resultant particles were verified to have higher quality in terms of particles sizes and size distribution, few satellites, and smooth surface [53]. Later, this modified coaxial process was successfully explored to round up the polymeric nanoparticles for better sustained release [34].

Going a further step along the previous development of modified coaxial electrospraying, the present study developed a new, modified coaxial electrospraying, in which a dilute ethylcellulose (EC) solution without solidifiable property was exploited as the shell working fluid to co-spray with a solidifiable core fluid containing a higher concentration of EC and drug. An anti-cancer drug, tamoxifen citrate (TAM), was utilized as a model drug to study the drug release kinetics. The morphology of the created particles, the thicknesses of the nanocoatings, and their performances in manipulating the drug sustained release kinetics were investigated in detail.

2. Materials and Methods

2.1. Materials

TAM (purity of 98%, white crystalline powders) was bought from Hua-Shi Pharmacy (Shanghai, China). EC was obtained from Shandong Fine Chemical Co., Ltd. (Jinan, China). Dichloromethane (DCM) and anhydrous ethanol were purchased from Shanghai Chemical Analysis Factory (Shanghai, China). All other components are analytical reagents, and water was double-distilled before use.

2.2. Modified Coaxial Electrospraying

A solution having solidifiable property was prepared by dissolving 10 g EC and 3 g TAM in a mixture of ethanol and DCM (1:1, v/v), meaning a concentration of 10% (w/v) EC and 3% (w/v) for them, respectively. This solution was exploited as the core working fluid. An unsolidifiable solution consisting of 2% (w/v) EC in a mixture of ethanol and DCM (1:1, v/v) was used as the shell fluid. Two sorts of nanoparticles, referred to as E1 and E2, were prepared at an applied voltage between 16–18 kV. For all preparations, the particle-collected distance was fixed at 15 cm. The electrospraying

processes were recorded using a digital camera (PowerShot A640, Tokyo, Japan). Other parameters are given in Table 1.

Table 1. Parameters about the electrosprayed nanoparticles.

No	Process	Voltage (kV)	Flow Rate (mL/h)		Morphology/Structure ^a	Drug Loading in the NPs (w/w%) ^b
			Core Fluid	Shell Fluid		
E1	Single-fluid	16	1.0		Irregular/Monolithic	23.1%
E2	Modified coaxial	18	1.0	0.3	Round/Core-shell	22.1%

^a The morphology and structure are experimental results. ^b The drug loading in the nanoparticles (NPs) (w/w%) is a theoretical value calculated according to the electrospraying conditions. Because electrospraying is essentially a physical drying process and tamoxifen citrate (TAM) has a boiling point of 140–144 °C without sublimation property, the drug encapsulation efficiency can be regarded as 100% [27,46].

2.3. Morphology of the Prepared Nanoparticles

Morphology and diameter of the fabricated NPs were studied and evaluated using a scanning electron microscope (SEM, Quanter 450, FEI, Hillsboro, OR, USA). The samples were sputtered with a thin layer of gold. Then the images were visualized and taken under an applied voltage of 20 kV. The average diameters of the NPs were determined by ImageJ software (National Institutes of Health, Bethesda, MD, USA) by randomly selecting about 50 particles. A transmission electron microscope (TEM, JEM 2100F, JEOL, Tokyo, Japan) was used to evaluate the inner structure of the prepared NPs.

2.4. Physical State of the Components and Their Compatibility

X-ray diffraction (XRD) patterns were recorded over the range 2θ from 5° to 60° using a Bruker X-ray diffractometer (Karlsruhe, Germany) with $\text{CuK}\alpha$ radiation. The X-rays were emitted at 40 kV and 30 mA. The presence of components, physical/chemical interactions, and drug–excipient compatibility were evaluated by using a Spectrum 100 FTIR Spectrometer (PerkinElmer, Waltham, MA, USA) at a range of 500–4000 cm^{-1} at a resolution of 2 cm^{-1} .

2.5. In Vitro Dissolution Tests

The drug release profiles from the NPs were assessed using a paddle method according to the Chinese Pharmacopoeia (2015 Edition). A weight of 100 mg NPs was placed into 900 mL physiological saline (pH = 7.0). The dissolution media were kept at 37 °C and a rotation rate of 50 rpm. At predetermined time points, a 5.0-mL aliquot was withdrawn and 5.0 mL of fresh physiological saline was added. The amounts of TAM released were measured at $\lambda_{\text{max}} = 272 \text{ nm}$ using a UV-VIS spectrophotometer (UV-2102PC, Unico Instrument Co. Ltd., Shanghai, China). The experimental results were reported as mean \pm standard deviation. All experiments were repeated six times.

3. Results and Discussion

3.1. Implementation of the Modified Coaxial Electrospraying

A schematic showing the main components of a modified coaxial system is given in Figure 1. Just as a coaxial electrospraying system or even a traditional single-fluid electrospraying system [54–56], the modified coaxial system, as an electrohydrodynamic atomization (EHDA) place, has the prerequisite four parts: A power supply for “electro-”, two syringe pumps for “hydro-”, a spraying head for the beginning of “dynamic” process, and a collector for collecting the resultant products of “atomization”. Other auxiliary parts (such as lights/camera/personal computer for observing the working processes, hot air blower for helping solidification) can be added to the system when they are necessary for a successful preparation of electrosprayed solid particles [57,58].

Among the four necessary parts, the spraying head is the most important section because it is a convergent point of electrical energy and fluid (or fluids), and it has the important role of guiding the working fluid (or fluids) into the electrical field for implementing an electrospraying process [59–61].

Thus, it is common sense that the working processes are often termed by the structures of the spraying heads. For example, a coaxial electrospaying is named due to a concentric spraying head that is utilized to organize the two working fluids. A side-by-side electrospaying (or electrospinning) is called because a side-by-side spraying head (or spinneret) is exploited to lead the double fluids into the electrical field in a side-by-side manner [62–64]. Shown in Figure 2 are the contents about the design (a), digital image (b), and connection with two syringes that can be utilized to hold the shell and core working fluids (c). The slight indenting of the core capillary about 0.1 mm should be favorable for a fine encapsulation of the shell fluid on the core fluid.

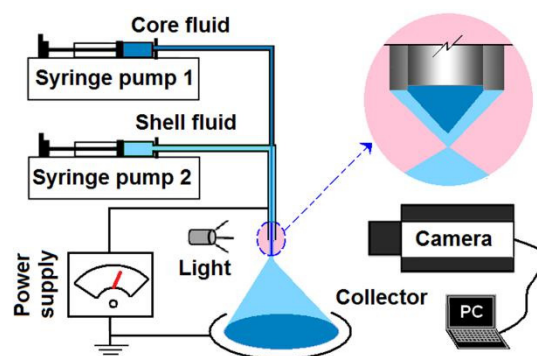


Figure 1. A schematic showing the main components of a modified coaxial system.

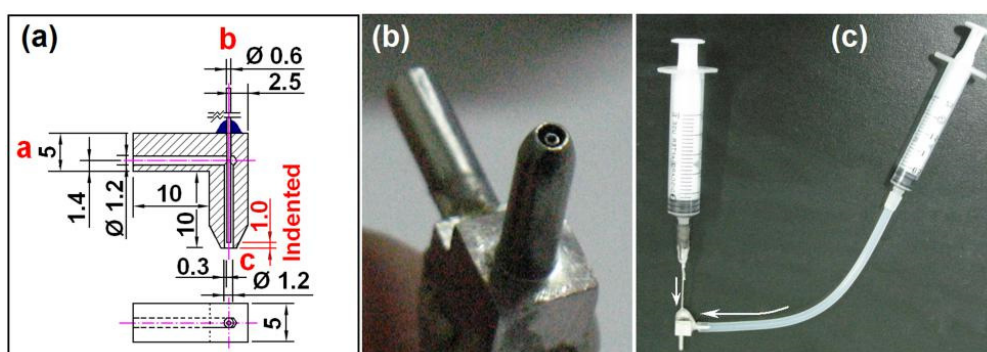


Figure 2. The homemade concentric spraying head for carrying out the modified coaxial processes: (a) Design details of the concentric spinneret with an indented section for fine encapsulation; (b) a digital picture about the concentric spraying head; (c) the connection of spraying head with two syringes.

The fabrication processes of the monolithic nanoparticles E1 and nanoparticles E2 with an EC coating are shown in Figure 3. When the shell working fluid of 2% (w/v) EC was turned off, the working process was essentially a single-fluid blending electrospaying. The core blended solutions had a nice, solidifiable property under the treatment of electrospaying. The process is shown in Figure 3a. Although 1×10^{-3} mg/mL methylene blue was added into the core fluid and the working fluid showed a blue color, the collected particles still had almost a white color. During the preparation process, the spraying head needed to be manually cleaned now and then because of the clogging from the semisolid substances. A typical image of them is shown in the upper-left inset image of Figure 3a. It should be attributed to the solvent mixture of ethanol and DCM, which are very easy to be evaporated and also the relatively high concentration of EC.

However, the fabrication processes of nanoparticles E2 were robust and continuous. Figure 3b shows a typical working process of the electrospaying. The classic three steps can be viewed clearly, i.e., the formation of a compound Taylor cone of the shell and core working fluids, a convergent point or a straight fluid jet, and a Coulomb explosion region showing the repelling and division of the charged liquids until they were solidified to reach the collector. A typical compound Taylor cone can

be recorded under a magnification of 12 with an opposite light source and the additive methylene blue as a color marker, which is given in the lower-right inset of Figure 3b.

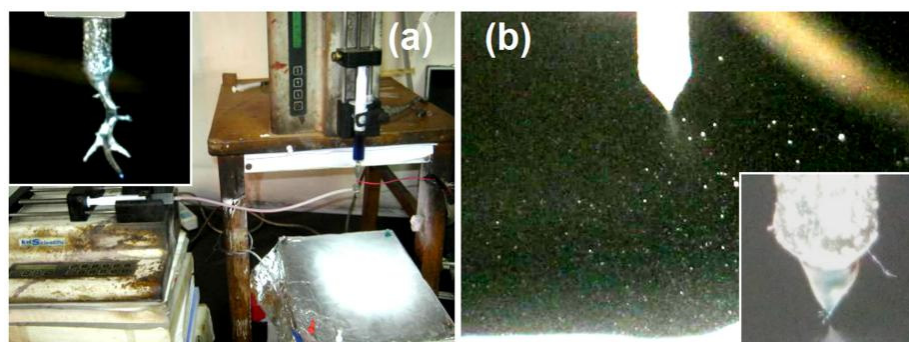


Figure 3. Observations about the modified coaxial electrospaying: (a) A digital picture about the whole apparatus and the preparation of monolithic nanoparticles E1, the upper-left inset showing a clogging phenomenon when the core EC-TAM blended fluid was subjected to electrospaying alone. (b) A digital image exhibiting the preparation process of nanoparticles E2 having an EC coating, the lower-right inset showing a typical compound Taylor cone.

3.2. The Morphology and Nanocoating Structure Studies

Just as anticipated, the monolithic nanoparticles E1 prepared using the single-fluid blended electrospaying showed a flat image with a center indented region, which is exhibited in Figure 4a. Meanwhile, there were many satellites clinging on the electrospayed particles. The estimated diameters of over 50 particles had an average value of $1.34 \pm 0.27 \mu\text{m}$. Apparently, these particles had a poor quality in terms of the shape, surface smoothness, and the uniform size distribution. The manual intervention on the preparation processes, the clogging phenomena, and also the unstable evaporation of DCM and ethanol co-acted to create these “ugly” nanoproducts. In sharp contrast, the prepared nanoparticles E2 with EC coating show a high quality in Figure 4b. These particles had a round morphology, a smooth surface, and also a relatively uniform size distribution of $0.87 \pm 0.14 \mu\text{m}$. Meanwhile, the numbers of satellites were very small.

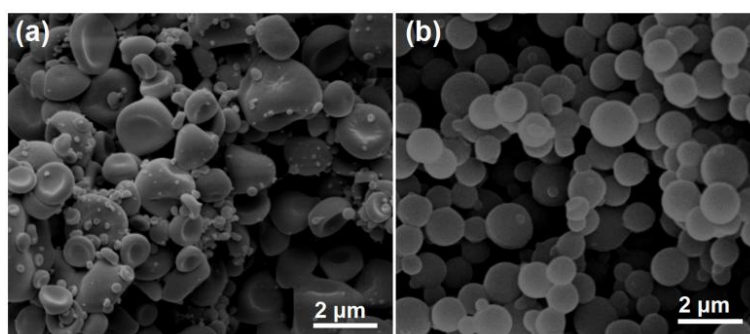


Figure 4. The SEM images of the prepared monolithic NPs using a single-fluid blended electrospaying (a) and NPs with EC coating using the modified coaxial electrospaying (b).

To evaluate the inner structures of those electrospayed particles, TEM images were achieved and are shown in Figure 5. The monolithic NPs E1 prepared from the single-fluid blended electrospaying had an irregular shape with uneven gray levels (Figure 5a). The gray levels of TEM images under a bright field resulted from three sections, i.e., the element, the density, and the thickness. Apparently, the indented sections in the particles often had a small thickness and, thus, correspondingly had a lighter gray level. In contrast, nanoparticles E2 from the modified coaxial electrospaying processes had an obvious core-shell nanostructure (Figure 5b). The core sections had a heavier gray level than

the shell section, which should be attributed to the different thickness of them and also their densities. The drug molecules can be distributed in the voids of the entanglements among the EC molecules and, thus, they can elevate the density of core sections. The thickness of the shell sections was estimated about 10–70 nm. In some places, there were transition regions between the core and shell sections, as indicated by dash lines A and B in Figure 5b. This phenomenon suggests that some drug molecules might diffuse from the core fluids to the shell fluids during the electrospaying processes.

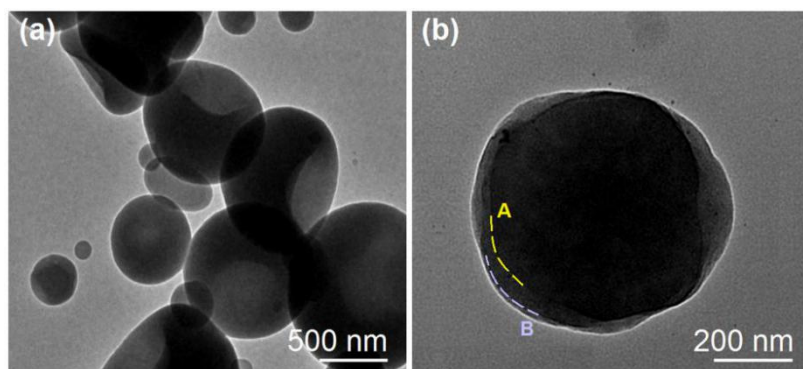


Figure 5. The TEM images of the of the prepared monolithic NPs using a single-fluid blended electrospaying (a) and NPs with EC coating using the modified coaxial electrospaying (b).

3.3. The Physical State of the Drug and the Compatibility of the Components

Shown in Figure 6 are XRD patterns of the crude materials (TAM and EC) and their nanoparticles E1 and E2. The patterns of TAM suggest that the raw TAM particles were typical crystalline due to the many sharp peaks responding to Bragg diffraction [49]. In contrast, the polymer EC had no responding peaks except two halos, suggesting that it was an amorphous material [47]. The nanoparticles from the two different electrospaying processes had a similar XRD pattern, just as the curve of EC. These phenomena indicate that the nanoparticles were amorphous nanocomposites. In other words, the drug TAM molecules co-existed with EC molecules in a molecularly dispersive state. The EC molecules acted as the space blocking agents to prevent the contact of TAM molecules and re-crystallization. The molecular dispersion state of EC and TAM molecules was a result of the extremely fast drying process of the electrospaying, by which the highly uniform state of TAM and EC in the working fluid was propagated into the solid nanoparticles, regardless of their morphologies and inner structures. Similar results are frequently reported about electrospun medicated nanofibers [25,38].

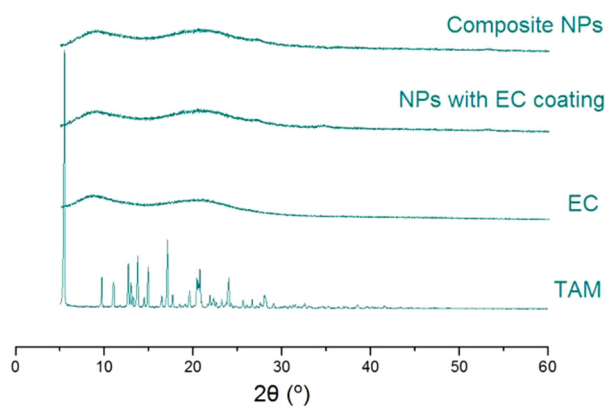


Figure 6. The XRD patterns of the crude materials and also their nanoparticles.

Attenuated total reflection ATR-FTIR spectra of the raw materials EC and TAM and also their nanoparticles are exhibited in Figure 7. The most important characteristic peak of TAM was at

1737 cm^{-1} , which was a response from the $-\text{C}=\text{O}$ groups. As for the EC, the strongest characteristic responses were at 1102 and 1063 cm^{-1} . In their electrospayed composite, NPs E1 and NPs E2 with EC coating, many peaks of the TAM were significantly decreased or even disappeared, which suggested that EC and TAM had good compatibility. This can be expected from their molecular formula. In a TAM molecule, there are three $-\text{C}=\text{O}$ groups and three benzene rings. The $-\text{C}=\text{O}$ groups can easily form hydrogen bonds with the $-\text{OH}$ groups in the EC molecules. Meanwhile, the benzene rings can interact with long carbon chains of EC molecules through the hydrophobic interactions. Thus, these second interactions should do favor to the fine compatibility of EC and TAM and also increase the physical stability of the prepared nanoparticles.

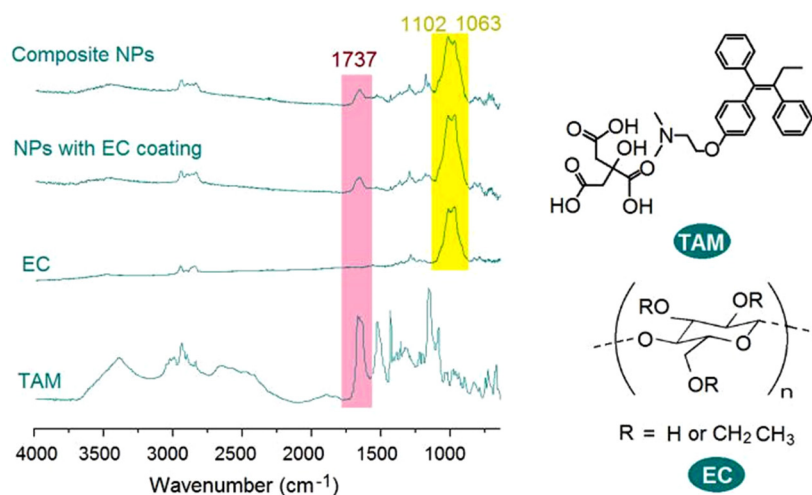


Figure 7. The attenuated total reflection (ATR)-FTIR spectra of the crude materials (EC and TAM) and also their nanoparticles and the molecular formula of TAM and EC.

3.4. The Functional Performances of the Nanocoating on the Drug Sustained Release Kinetics

The drug sustained release profiles of the two types of NPs are included in Figure 8. Figure 8a,b shows the accumulative drug release (%) as a function of drug release time and the time needed for finishing a certain percentage of drug loaded in the created nanoparticles, respectively. The performances can be compared mainly from two aspects: The initial burst release amount and the subsequent sustained release time period. Composite NPs E1 provided a $34.2 \pm 4.5\%$ release at the first hour, a typical initial burst release because of a value over 30% [48]. In comparison, NPs with EC coating released only $3.4 \pm 2.1\%$ (Figure 8a). From another angle, a content of 30% release took 0.88 h and 7.58 h for NPs E1 and E2, respectively (Figure 8b). Thus, the NPs with EC coating completely eliminated the initial burst release due to the blank shell EC layer coating. At the sampling time point of 20 h, NPs E1 released $93.3 \pm 5.5\%$ of their cargoes, whereas NPs E2 released $92.7 \pm 5.1\%$ of the loaded drug at the time point of 30 h. The NPs with EC coating were able to provide a longer time period of drug sustained release. This can be also reflected from the time needed for finishing a release of 50% and 90%. NPs E1 needed only 1.89 h and 16.85 h, respectively, whereas NPs with EC coating took 12.79 h and 28.74 h, respectively. Additionally, the release data of NPs E2 can be regressed using the linear equation, i.e., $y = ax + b$. Shown in Figure 8a, the drug release percentage (Q) had a fine, linear relationship with the drug release time (t) with a high correlation coefficient $R = 0.9863$. The equation is $Q = 5.4261 + 2.9138t$. The linear release is very useful for accurately predicting the drug release profiles and, in turn, for the personal therapeutics in the future.

To disclose the influences of EC coating on the drug release kinetics, the release data of NPs E1 and E2 were treated using Peppas equation [65,66], i.e., $Q = kt^n$, where Q is the drug release amount, t is the release time, k is a constant, and n is an indicating constant about the drug release mechanism. The common knowledge is that $n \leq 0.45$ suggests a Fickian diffusion mechanism, $n \geq 0.9$ suggests an

erosion mechanism, and $0.45 \leq n \leq 0.90$ suggests a combined mechanism. The regressed equations for NPs E1 (Figure 9a) and E2 (Figure 9b) are $Q = 39.38t^{0.29}$ ($R = 0.9767$) and $Q = 3.96t^{0.98}$ ($R = 0.9958$), respectively. Thus, NPs E1 released the drug through a typical Fickian diffusion mechanism, suggested by an n value of $0.29 < 0.45$. This can be expected because EC is an insoluble drug and the drug molecules must gradually penetrate and diffuse through the EC matrices to reach the bulk dissolution media. However, the drug release mechanism for the NPs E2 with EC coating was suggested to be an erosion mechanism, owing to a value of $n = 0.98 > 0.90$. This is not true. The reason should be that the prerequisite condition of Peppas equation is that the drug molecules must be uniformly distributed all over the matrices. Thus, the blank EC shell-layer coating in NPs E2 makes the Peppas equation invalid here. In other word, Peppas equation is useful for predicting drug release mechanism from a certain matrix but is invalid for predicting drug release mechanism from the complex nanostructures. This case was also demonstrated by the core-shell, fiber-based drug depots [47].

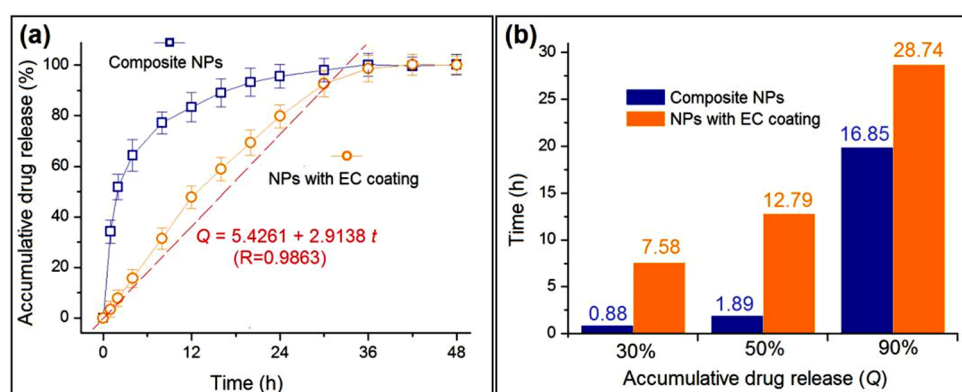


Figure 8. The in vitro drug sustained release performances: (a) Accumulative drug release as a function of drug release time and (b) the needed time for reaching a certain percentage of drug loaded in the created nanoparticles.

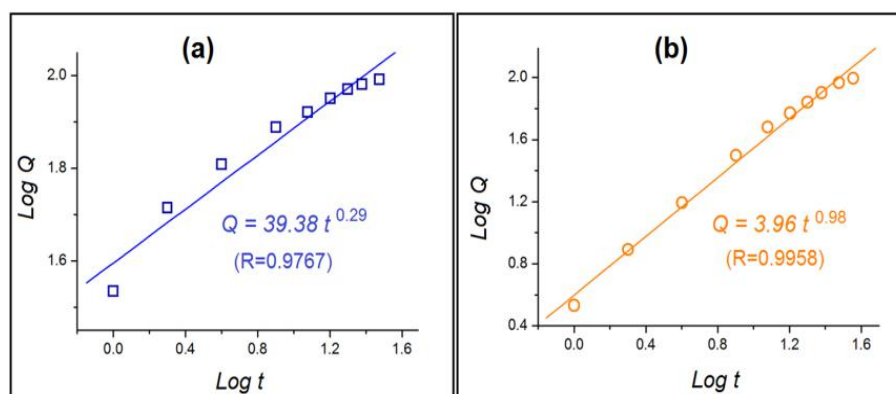


Figure 9. The regressed equations of the drug release data of nanoparticles E1 and E2 based on the Peppas equation: (a) Composite NPs E1, (b) NPs with EC coating E2.

3.5. The Mechanism of EC Coating in Adjusting the Drug Release Kinetics and the Related Perspectives

Figure 10 is a diagram explaining the functions of the ultra-thin EC coating in manipulating the drug release behaviors. For the composite NPs E1 to form the single-fluid blending electrospaying, the drug molecules are uniformly distributed within the EC matrix. Although it is soluble in a variety of organic solvents and is convenient for treating, EC is insoluble in water. This unique property has made EC become a popular coating agent for achieving oral, sustained release pharmaceutical formulations, such as tablets and pellets [67–69]. Thus, in the present electrospayed NPs, the uniform distribution in NPs E1 inevitably resulted in a typical diffusion process for the drug release.

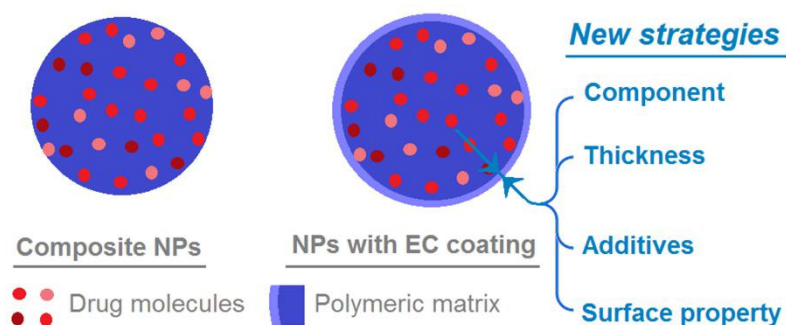


Figure 10. A diagram showing the functions of the ultra-thin EC coating in manipulating the drug release behaviors, and the new strategies that can be developed from the present protocols for the further investigations.

When an EC blank coating is applied on the surface of the composite NPs, it can adjust the drug release performances from the following three aspects. Firstly, the blank coating removes the presence of drug molecules on the NPs' surface, which is very useful for eliminating the initial burst release. Secondly, the blank coating provides an additional barrier for the inner drug molecules to diffuse into the bulk solution, which is useful for prolonging the drug release time period. Thirdly, the blank EC surface should have a high hydrophobic property, which would increase the diffusion resistances of both the water molecules penetrating into the NPs and the drug molecules diffusing out from the particles to the bulk solution. Thus, the EC layer coating can modify the drug release behaviors from the NPs profoundly.

In this nano-era, NPs from all kinds of raw materials have been tried to provide the designed drug-controlled release profiles, such as polymer, lipid, inorganic, and magnetic substances [11,70–74]. Based on the present protocols, there are some new strategies that can be applied for developing novel polymer coating NPs. For example, a wide variety of raw materials can be explored to modify the traditional NPs through electrospraying [75–77]. In this study, the coating material was EC but, apparently, many other polymers and lipids can be similarly utilized to coat the medicated NPs. Meanwhile, the thicknesses of shell blank layer can be exploited as a key parameter to adjust the drug release profiles, which in turn can be manipulated by the flow rate of the shell working fluid and also its polymeric concentrations. Additives such as the pore-forming agents may be also added into the surface-coating layer, and the shell layer's surface property may be also manipulated about its hydrophobic and hydrophilic properties for a further fine tuning of drug release profile. Particularly, some popular inorganic NPs may be improved about their biocompatibility when they are coated with polymers or lipids [78,79].

4. Conclusions

A modified, coaxial electrospraying was successfully implemented to form an ultra-thin EC shell layer on the medicated EC-TAM core. The diluted shell working fluid containing 2% (w/v) EC made the modified coaxial processes more continuous and robust. Meanwhile, the generated NPs with EC coating had a higher quality than the monolithic ones from the single-fluid blended process in terms of their shapes, surface smoothness, smaller size, and the uniform size distribution. XRD patterns suggested that the drug TAM presented in all the NPs in an amorphous state, owing to the good compatibility between TAM and EC. In vitro dissolution tests showed that the NPs with EC coating took time periods of 7.58 h, 12.79 h, and 28.74 h for an accumulative release of 30%, 50%, and 90% of the loaded drug, respectively. These data demonstrated that the NPs with EC coating were able to offer a better drug sustained release performance than the monolithic composite NPs, whose corresponding time periods were 0.88 h, 1.89 h, and 16.85 h. The drug molecules released from the composite NPs through a typical Fickian diffusion mechanism, whereas the drug released from the NPs with

EC coating did not obey the Peppas equation. The EC coating changed the drug molecule diffusion behaviors profoundly, which will be further investigated.

Author Contributions: Conceptualization, X.-J.L., X.-L.L., W.-D.H., and D.-G.Y.; experiments, W.-D.H., X.X., and H.-L.W.; writing-original draft preparation, W.-D.H., J.-X.H., and X.-H.Z.; writing-review and editing, all authors; supervision, X.-L.L. and D.-G.Y.; project administration, X.-J.L., X.-L.L., and D.-G.Y. All authors have read and agreed to the published version of the manuscript.

Funding: The National Natural Science Foundation of China (Nos. 51803121 & 51402099); the Technical Innovation Project (Major Project) of Hubei, China (2016ACA176); University-Industry Collaborative Education Program (201902313008); Hubei Provincial Department of Education (B2013060); The Hubei Key Laboratory Foundation (2012107& 2013105); and Shanghai Natural Science Foundation (No. 20ZR1439000) are appreciated.

Conflicts of Interest: The authors declare no conflict of interest.

References

1. Castanheira, E.J.; Correia, T.R.; Rodrigues, J.M.M.; Mano, J.F. Novel biodegradable laminarin microparticles for biomedical applications. *Bull. Chem. Soc. Jpn.* **2020**, *93*, 713–719. [[CrossRef](#)]
2. Hassani Besheli, N.; Mottaghitalab, F.; Eslami, M.; Gholami, M.; Kundu, S.C.; Kaplan, D.L.; Farokhi, M. Sustainable release of vancomycin from silk fibroin nanoparticles for treating severe bone infection in rat tibia osteomyelitis model. *ACS Appl. Mater. Interfaces* **2017**, *9*, 5128–5138. [[CrossRef](#)]
3. Andreani, T.; Fangueiro, J.F.; Jose, S.; Santini, A.; Silva, A.M.; Souto, E.B. Hydrophilic polymers for modified-release nanoparticles: A review of mathematical modelling for pharmacokinetic analysis. *Curr. Pharm. Des.* **2015**, *21*, 3090–3096. [[CrossRef](#)] [[PubMed](#)]
4. Soroushnaei, A.; Ganji, F.; Vasheghani-Farahani, E.; Mobedi, H. Development and evaluation of an anti-epileptic oral fast-dissolving film with enhanced dissolution and in vivo permeation. *Curr. Drug Deliv.* **2018**, *15*, 1294–1304. [[CrossRef](#)] [[PubMed](#)]
5. Salar-Behzadi, S.; Corzo, C.; Schaden, L.; Laggner, P.; Zimmer, A. Correlation between the solid state of lipid coating and release profile of API from hot melt coated microcapsules. *Int. J. Pharm.* **2019**, *565*, 569–578. [[CrossRef](#)] [[PubMed](#)]
6. Bannow, J.; Koren, L.; Salar-Behzadi, S.; Löbmann, K.; Zimmer, A.; Rades, T. Hot melt coating of amorphous carvedilol. *Pharmaceutics* **2020**, *12*, 519. [[CrossRef](#)]
7. Keser, S.; Timpe, C.; Zimmer, A. Development and evaluation of taste-masked pediatric minitab formulations with bitter model drugs. *Int. J. Pharm.* **2018**, *536*, 512. [[CrossRef](#)]
8. Tan, J.M.; Saifullah, B.; Kura, A.U.; Fakurazi, S.; Hussein, M.Z. Incorporation of levodopa into biopolymer coatings based on carboxylated carbon nanotubes for pH-dependent sustained release drug delivery. *Nanomaterials* **2018**, *8*, 389. [[CrossRef](#)]
9. Paudel, A.; Gomes Lopes, D.; Garsuch, V.; Becker, K.; Zimmer, A.; Salar-Behzadi, S. Improving the granule strength of roller-compacted ibuprofen sodium for hot-melt coating processing. *Int. J. Pharm.* **2016**, *510*, 285–295.
10. Demiri, V.; Stranzinger, S.; Rinner, P.; Piller, M.; Sacher, S.; Lingitz, J.; Khinast, J.; Salar-Behzadi, S. Gluing pills technology: A novel route to multilayer tablet manufacturing. *Int. J. Pharm.* **2018**, *548*, 672–681. [[CrossRef](#)]
11. Li, Q.; Cai, T.; Huang, Y.; Xia, X.; Cole, S.P.C.; Cai, Y. A review of the structure, preparation, and application of NLCs, PNPs, and PLNs. *Nanomaterials* **2017**, *7*, 122. [[CrossRef](#)] [[PubMed](#)]
12. Muller, K.; Bugnicourt, E.; Latorre, M.; Jorda, M.; Sanz, Y.; Lagaron, J.M.; Schmid, M. Review on the processing and properties of polymer nanocomposites and nanocoatings and their applications in the packaging, automotive and solar energy fields. *Nanomaterials* **2017**, *7*, 74. [[CrossRef](#)] [[PubMed](#)]
13. Wu, S.; Zellnitz, S.; Mercuri, A.; Salar-Behzadi, S.; Bresciani, M.; Eleonore, F. An in vitro and in silico study of the impact of engineered surface modifications on drug detachment from model carriers. *Int. J. Pharm.* **2016**, *513*, 109–117. [[CrossRef](#)] [[PubMed](#)]
14. Alshetaibi, A.S.; Almutairy, B.K.; Tiwari, R.V.; Morott, J.T.; Alshehri, S.M.; Feng, X.; Alsulays, B.B.; Park, J.B.; Zhang, F.; Repka, M.A. Preparation and evaluation of hot-melt extruded patient-centric ketoprofen mini-tablets. *Curr. Drug Deliv.* **2016**, *13*, 730–741. [[CrossRef](#)] [[PubMed](#)]
15. Masood, F. Polymeric nanoparticles for targeted drug delivery system for cancer therapy. *Mater. Sci. Eng. C Mater.* **2016**, *60*, 569–578. [[CrossRef](#)]

16. Bock, N.; Dargaville, T.R.; Woodruff, M.A. Electrospinning of polymers with therapeutic molecules: State of the art. *Prog. Polym. Sci.* **2012**, *37*, 1510–1551. [[CrossRef](#)]
17. Wang, W.; Mattoussi, H. Engineering the bio-nano interface using a multifunctional coordinating polymer coating. *Acc. Chem. Res.* **2020**, *53*, 1124–1138. [[CrossRef](#)]
18. Karimi, Z.; Karimi, L.; Shokrollahi, H. Nano-magnetic particles used in biomedicine: Core and coating materials. *Mater. Sci. Eng. C* **2013**, *33*, 2465–2475. [[CrossRef](#)]
19. Souto, E.B.; Silva, G.F.; Dias-Ferreira, J.; Zielinska, A.; Ventura, F.; Durazzo, A.; Lucarini, M.; Novellino, E.; Santini, A. Nanopharmaceutics: Part I-Clinical trials legislation and good manufacturing practices (GMP) of nanotherapeutics in the EU. *Pharmaceutics* **2020**, *12*, 146. [[CrossRef](#)]
20. Yeung, A.W.K.; Souto, E.B.; Durazzo, A.; Lucarini, M.; Santini, A. Big impact of nanoparticles: Analysis of the most cited nanopharmaceuticals and nanonutraceuticals research. *Curr. Res. Biotechnol.* **2020**, *2*, 53–63. [[CrossRef](#)]
21. Souto, E.B.; Silva, G.F.; Dias-Ferreira, J.; Zielinska, A.; Ventura, F.; Durazzo, A.; Lucarini, M.; Novellino, E.; Santini, A. Nanopharmaceutics: Part II-Production scales and clinically compliant production methods. *Nanomaterials* **2020**, *10*, 455. [[CrossRef](#)]
22. Ghosh Chaudhuri, R.; Paria, S. Core/shell nanoparticles: Classes, properties, synthesis mechanisms, characterization, and applications. *Chem. Rev.* **2012**, *112*, 2373–2433. [[CrossRef](#)] [[PubMed](#)]
23. Vass, P.; Szabó, E.; Domokos, A.; Hirsch, E.; Galata, D.; Farkas, B.; Marosi, G. Scale-up of electrospinning technology: Applications in the pharmaceutical industry. *Wiley Interdiscip. Rev. Nanomed. Nanobiotechnol.* **2020**, *12*, e1611. [[CrossRef](#)] [[PubMed](#)]
24. Sill, T.J.; von Recum, H.A. Electrospinning: Applications in drug delivery and tissue engineering. *Biomaterials* **2008**, *29*, 1989–2006. [[CrossRef](#)] [[PubMed](#)]
25. Wang, M.; Yu, D.G.; Li, X.; Williams, G.R. The development and bio-applications of multifluid electrospinning. *Mater. Highlights* **2020**, *1*, 1.
26. Singh, A.; Rath, G.; Singh, R.; Goyal, A.K. Nanofibers: An effective tool for controlled and sustained drug delivery. *Curr. Drug Deliv.* **2018**, *15*, 155–166. [[CrossRef](#)]
27. Sequeira, R.S.; Miguel, S.P.; Cabral, C.S.; Moreira, A.F.; Ferreira, P.; Correia, I.J. Development of a poly (vinyl alcohol)/lysine electrospun membrane-based drug delivery system for improved skin regeneration. *Int. J. Pharm.* **2019**, *570*, 118640. [[CrossRef](#)]
28. Miguel, S.P.; Sequeira, R.S.; Moreira, A.F.; Cabral, C.S.; Mendonca, A.G.; Ferreira, P.; Correia, I.J. An overview of electrospun membranes loaded with bioactive molecules for improving the wound healing process. *Eur. J. Pharm. Biopharm.* **2019**, *139*, 1–22. [[CrossRef](#)]
29. Vlachou, M.; Kikionis, S.; Siamidi, A.; Tragou, K.; Kapoti, S.; Ioannou, E.; Roussis, V.; Tsoinis, A. Fabrication and characterization of electrospun nanofibers for the modified release of the chronobiotic hormone melatonin. *Curr. Drug Deliv.* **2019**, *16*, 79–85. [[CrossRef](#)]
30. Torres-Martínez, E.J.; Cornejo Bravo, J.M.; Serrano Medina, A.; Pérez González, G.L.; Villarreal Gómez, L.J. A summary of electrospun nanofibers as drug delivery system: Drugs loaded and biopolymers used as matrices. *Curr. Drug Deliv.* **2018**, *15*, 1360–1374.
31. Fan, W.; Zhang, X.L.; Li, C.J. Functional fibrous compositions: Applications and perspectives. *Composit. Coummun.* **2019**, *15*, 68–75. [[CrossRef](#)]
32. Song, W.; Zhao, B.; Wang, C.; Lu, X.F. Electrospun nanofibrous materials: A versatile platform for enzyme mimicking and their sensing applications. *Composit. Coummun.* **2019**, *12*, 1–13. [[CrossRef](#)]
33. He, Y.; Jin, Y.; Wang, X.; Yao, S.; Li, Y.; Wu, Q.; Liu, H. An antimicrobial peptide-loaded gelatin/chitosan nanofibrous membrane fabricated by sequential layer-by-layer electrospinning and electrospinning techniques. *Nanomaterials* **2018**, *8*, 327. [[CrossRef](#)] [[PubMed](#)]
34. Wang, K.; Wen, H.F.; Yu, D.G.; Yang, Y.; Zhang, D.F. Electrospun hydrophilic nanocomposites coated with shellac for colon-specific delayed drug delivery. *Mater. Des.* **2018**, *143*, 248–255. [[CrossRef](#)]
35. Higuchi, J.; Fortunato, G.; Woźniak, B.; Chodara, A.; Domaschke, S.; Meczynskawielgosz, S.; Łojkowski, W. Polymer membranes sonocoated and electrospun with nano-hydroxyapatite for periodontal tissues regeneration. *Nanomaterials* **2019**, *9*, 1625. [[CrossRef](#)] [[PubMed](#)]

36. Smeets, A.; Lo Re, I.; Clasen, C.; Van den Mooter, G. Fixed dose combinations for cardiovascular treatment via coaxial electrospinning: Coated amorphous solid dispersion particles. *Int. J. Pharm.* **2020**, *577*, 118949. [[CrossRef](#)]
37. Chuysinuan, P.; Pengsuk, C.; Lirdprapamongkol, K.; Techasakul, S.; Svasti, J.; Nooeaid, P. Enhanced structural stability and controlled drug release of hydrophilic antibiotic-loaded alginate/soy protein isolate core-sheath fibers for tissue engineering applications. *Fiber. Polym.* **2019**, *20*, 1–10. [[CrossRef](#)]
38. Yu, D.G.; Wang, M.; Li, X.; Liu, X.; Zhu, L.M.; Annie Bligh, S.W. Multifluid electrospinning for the generation of complex nanostructures. *Wiley Interdiscip. Rev. Nanomed. Nanobiotechnol.* **2020**, *12*, e1601. [[CrossRef](#)] [[PubMed](#)]
39. Wang, M.; Wang, K.; Yang, Y.; Liu, Y.; Yu, D.G. Electrospun environment remediation nanofibers using unspinnable liquids as the sheath fluids: A review. *Polymers* **2020**, *12*, 103. [[CrossRef](#)]
40. Yang, Y.; Chang, S.; Bai, Y.; Du, Y.; Yu, D.G. Discrete drug distributions within electrospun tri-layer core-shell nanofibers for accurate dual-stage release. *Carbohydr. Polym.* **2020**, *243*, 116477. [[CrossRef](#)]
41. Wang, M.; Hou, J.; Yu, D.G.; Li, S.; Zhu, J.; Chen, Z. Electrospun tri-layer nanodepots for sustained release of acyclovir. *J. Alloy. Compd.* **2020**, *846*, 156471. [[CrossRef](#)]
42. Moghe, A.K.; Gupta, B.S. Co-axial electrospinning for nanofiber structures: Preparation and applications. *Polym. Rev.* **2008**, *48*, 353–377. [[CrossRef](#)]
43. Javadi, A.; Solouk, A.; Nazarpak, M.H.; Bagheri, F. Surface engineering of titanium-based implants using electrospinning and dip coating methods. *Mater. Sci. Eng. C* **2019**, *99*, 620–630. [[CrossRef](#)] [[PubMed](#)]
44. Yoon, J.; Yang, H.S.; Lee, B.S.; Yu, W.R. Recent progress in coaxial electrospinning: New parameters, various structures, and wide applications. *Adv. Mater.* **2018**, *30*, 1704765. [[CrossRef](#)] [[PubMed](#)]
45. Paezvelez, C.; Castromayorga, J.L.; Dussan, J. Effective gold biosorption by electrospun and electrospayed bio-composites with immobilized lysinibacillus sphaericus CBAM5. *Nanomaterials* **2020**, *10*, 408. [[CrossRef](#)] [[PubMed](#)]
46. Wang, M.; Hai, T.; Feng, Z.; Yu, D.G.; Yang, Y.; Annie Bligh, S. The relationships between the working fluids, process characteristics and products from the modified coaxial electrospinning of zein. *Polymers* **2019**, *11*, 1287. [[CrossRef](#)]
47. Huang, C.K.; Zhang, K.; Gong, Q.; Yu, D.G.; Wang, J.; Tan, X.; Quan, H. Ethylcellulose-based drug nano depots fabricated using a modified triaxial electrospinning. *Int. J. Biol. Macromol.* **2020**, *152*, 68–76. [[CrossRef](#)]
48. Hou, J.; Yang, J.; Zheng, X.; Wang, M.; Liu, Y.; Yu, D.G. A nanofiber-based drug depot with high drug loading for sustained release. *Int. J. Pharm.* **2020**, *583*, 119397. [[CrossRef](#)]
49. Wang, K.; Wang, P.; Wang, M.; Yu, D.G.; Wan, F.; Bligh, S.W.A. Comparative study of electrospun crystal-based and composite-based drug nano depots. *Mater. Sci. Eng. C* **2020**, *113*, 110988. [[CrossRef](#)]
50. Zhao, K.; Wang, W.; Yang, Y.; Wang, K.; Yu, D.G. From taylor cone to solid nanofiber in tri-axial electrospinning: Size relationships. *Results Phys.* **2019**, *15*, 102770. [[CrossRef](#)]
51. Chang, S.; Wang, M.; Zhang, F.; Liu, Y.; Liu, X.; Yu, D.G.; Shen, H. Sheath-separate-core nanocomposites fabricated using a trifluid electrospinning. *Mater. Des.* **2020**, *192*, 108782. [[CrossRef](#)]
52. Loscertales, I.G.; Barrero, A.; Guerrero, I.; Cortijo, R.; Marquez, M.; Ganan-Calvo, A.M. Micro/nano encapsulation via electrified coaxial liquid jets. *Science* **2002**, *295*, 1695–1698. [[CrossRef](#)] [[PubMed](#)]
53. Liu, Z.P.; Zhang, L.L.; Yang, Y.Y.; Wu, D.; Jiang, G.; Yu, D.G. Preparing composite nanoparticles for immediate drug release by modifying electrohydrodynamic interfaces during electrospinning. *Powder Technol.* **2018**, *327*, 179–187. [[CrossRef](#)]
54. Tapia-Hernández, J.A.; del-Toro-Sánchez, C.L.; Cinco-Moroyoqui, F.J.; Ruiz-Cruz, S.; Juárez, J.; Castro-Enríquez, D.D.; Barreras-Urbina, C.G.; López-Ahumada, G.A.; Rodríguez-Felix, F. Gallic acid-loaded zein nanoparticles by electrospinning process. *J. Food Sci.* **2019**, *84*, 818–831. [[CrossRef](#)] [[PubMed](#)]
55. Tapia-Hernandez, J.A.; Torres-Chavez, P.I.; Ramirez-Wong, B.; Rascon-Chu, A.; Plascencia-Jatomea, M.; Barreras-Urbina, C.G.; Rangel-Vázquez, N.A.; Rodríguez-Felix, F. Micro-and nanoparticles by electrospinning: Advances and applications in foods. *J. Agric. Food Chem.* **2015**, *63*, 4699–4707. [[CrossRef](#)] [[PubMed](#)]
56. Shams, T.; Parhizkar, M.; Illangakoon, U.E.; Orlu, M.; Edirisinghe, M. Core/shell microencapsulation of indomethacin/paracetamol by co-axial electrohydrodynamic atomization. *Mater. Des.* **2017**, *136*, 204–213. [[CrossRef](#)]

57. Mehta, P.; Haj-Ahmad, R.; Rasekh, M.; Arshad, M.S.; Smith, A.; van der Merwe, S.M.; Li, X.; Chang, M.W.; Ahmad, Z. Pharmaceutical biomaterial engineering via electrohydrodynamic atomization technologies. *Drug Discov. Today* **2017**, *22*, 157–165. [[CrossRef](#)]
58. Chakraborty, S.; Liao, I.C.; Adler, A.; Leong, K.W. Electrohydrodynamics: A facile technique to fabricate drug delivery systems. *Adv. Drug Deliver. Rev.* **2009**, *61*, 1043–1054. [[CrossRef](#)]
59. Parhizkar, M.; Reardon, P.J.T.; Knowles, J.C.; Browning, R.J.; Stride, E.; Pedley, R.B.; Grego, I.; Edirisinghe, M. Performance of novel high throughput multi electrospray systems for forming of polymeric micro/nanoparticles. *Mater. Des.* **2017**, *126*, 73–84. [[CrossRef](#)]
60. Tapia-Hernández, J.A.; Rodríguez-Félix, D.E.; Plascencia-Jatomea, M.; Rascón-Chu, A.; López-Ahumada, G.A.; Ruiz-Cruz, S.; Barreras-Urbina, C.G.; Rodríguez-Félix, F. Porous wheat gluten microparticles obtained by electrospray: Preparation and characterization. *Adv. Polym. Technol.* **2018**, *37*, 2314–2324. [[CrossRef](#)]
61. Nhat Nguyen, D.; Clasen, C.; van den Mooter, G. Pharmaceutical applications of electrospraying. *J. Pharm. Sci.* **2016**, *105*, 2601–2620. [[CrossRef](#)] [[PubMed](#)]
62. Wang, P.; Wang, M.; Wan, X.; Zhou, H.; Zhang, H.; Yu, D.G. Dual-stage release of ketoprofen from electrosprayed core-shell hybrid polyvinyl pyrrolidone/ethyl cellulose nanoparticles. *Mater. Highlights* **2020**, *1*, 2.
63. Kadivar, N.; Tavanai, H.; Allafchian, A. Fabrication of cellulose nanoparticles through electrospraying. *IET Nanobiotechnol.* **2018**, *12*, 807–813. [[CrossRef](#)] [[PubMed](#)]
64. Wang, M.; Li, D.; Li, J.; Li, S.; Chen, Z.; Yu, D.G.; Liu, Z.; Guo, J.Z. Electrospun Janus zein–PVP nanofibers provide a two-stage controlled release of poorly water-soluble drugs. *Mater. Des.* **2020**. [[CrossRef](#)]
65. Siepmann, J.; Peppas, N.A. Higuchi equation: Derivation, applications, use and misuse. *Int. J. Pharm.* **2011**, *418*, 6–12. [[CrossRef](#)]
66. Peppas, P. Analysis of Fickian and non-Fickian drug release from polymers. *Pharm. Acta Helvetica* **1985**, *60*, 110–111.
67. Chaerunisaa, A.Y.; Ali, R.; Korber, M.; Bodmeier, R. Quantification of porogen effect on the drug release from single-and multi-layered ethylcellulose coated pellets containing single or combined drugs. *Int. J. Pharm.* **2020**, *577*, 119050. [[CrossRef](#)]
68. Ni, B.; Liu, M.; Lue, S. Multifunctional slow-release urea fertilizer from ethylcellulose and superabsorbent coated formulations. *Chem. Eng. J.* **2009**, *155*, 892–898. [[CrossRef](#)]
69. Pearnchob, N.; Bodmeier, R. Coating of pellets with micronized ethylcellulose particles by a dry powder coating technique. *Int. J. Pharm.* **2003**, *268*, 1–11. [[CrossRef](#)]
70. Fernandes, N.; Rodrigues, C.F.; Moreira, A.F.; Correia, I.J. Overview of the application of inorganic nanomaterials in cancer photothermal therapy. *Biomater. Sci.* **2020**, *8*, 2990–3020. [[CrossRef](#)]
71. Cazarescortes, E.; Nerantzaki, M.; Fresnais, J.; Wilhelm, C.; Griffete, N.; Menager, C. Magnetic nanoparticles create hot spots in polymer matrix for controlled drug release. *Nanomaterials* **2018**, *8*, 850. [[CrossRef](#)] [[PubMed](#)]
72. Phan, T.T.; Huynh, T.; Manivasagan, P.; Mondal, S.; Oh, J. An up-to-date review on biomedical applications of palladium nanoparticles. *Nanomaterials* **2019**, *10*, 66. [[CrossRef](#)] [[PubMed](#)]
73. Darwish, M.S.A.; Kim, H.; Lee, H.; Ryu, C.; Young, L.J.; Yoon, J. Engineering core-shell structures of magnetic ferrite nanoparticles for high hyperthermia performance. *Nanomaterials* **2020**, *10*, 991. [[CrossRef](#)] [[PubMed](#)]
74. Moreira, A.F.; Rodrigues, C.F.; Reis, C.A.; Costa, E.C.; Correia, I.J. Gold-core silica shell nanoparticles application in imaging and therapy: A review. *Micropor. Mesopor. Mater.* **2018**, *270*, 168–179. [[CrossRef](#)]
75. Szczech, M.; Szczepanowicz, K. Polymeric core-shell nanoparticles prepared by spontaneous emulsification solvent evaporation and functionalized by the layer-by-layer method. *Nanomaterials* **2020**, *10*, 496. [[CrossRef](#)] [[PubMed](#)]
76. Prieto, C.; Lagaron, J.M. Nanodroplets of docosahexaenoic acid-enriched algae oil encapsulated within microparticles of hydrocolloids by emulsion electrospraying assisted by pressurized gas. *Nanomaterials* **2020**, *10*, 270. [[CrossRef](#)] [[PubMed](#)]
77. Ramoshernandez, J.A.; Ragazzosanchez, J.A.; Calderonsantoyo, M.; Ortizbasurto, R.I.; Prieto, C.; Lagaron, J.M. Use of electrosprayed agave Fructans as nanoencapsulating hydrocolloids for bioactives. *Nanomaterials* **2018**, *8*, 868. [[CrossRef](#)]

78. Jacinto, T.A.; Rodrigues, C.F.; Moreira, A.F.; Miguel, S.P.; Costa, E.C.; Ferreira, P.; Correia, I.J. Hyaluronic acid and vitamin E polyethylene glycol succinate functionalized gold-core silica shell nanorods for cancer targeted photothermal therapy. *Colloids Surf. B* **2020**, *188*, 110778. [[CrossRef](#)]
79. Rodrigues, C.F.; Reis, C.A.; Moreira, A.F.; Ferreira, P.; Correia, I.J. Optimization of gold core-mesoporous silica shell functionalization with TPGS and PEI for cancer therapy. *Micropor. Mesopor. Mater.* **2019**, *285*, 1–12. [[CrossRef](#)]



© 2020 by the authors. Licensee MDPI, Basel, Switzerland. This article is an open access article distributed under the terms and conditions of the Creative Commons Attribution (CC BY) license (<http://creativecommons.org/licenses/by/4.0/>).